View metadata, citation and similar papers at core.ac.uk
brought to you by CORE
provided by Xiamen University Institutional Repository

Microscopic interferometer for surface roughness measurement

Zhihua Ding
Guiying Wang
Zhijiang Wang, FELLOW SPIE
Chinese Academy of Sciences
Shanghai Institute of Optics and Fine Mechanics
P.O. Box 800-211
Shanghai 201800, China

Abstract. We describe a phase-shifting microscopic Mirau interferometer for measurement of surface roughness in which feedback control is implemented for shifter asymptotic adjustment. The actual height resolution of our instrument is of ~0.3 nm with a measurement accuracy of 0.5 nm. Comments on interferometer design, experimental examples, and error analysis are also given. *© 1996 Society of Photo-Optical Instrumentation Engineers.*

Subject terms: Mirau interferometer; profiler; roughness measurement; phase shifting.

Paper 34095 received Sep. 25, 1995; revised manuscript received Apr. 3, 1996; accepted for publication Apr. 4, 1996.

1 Introduction

In a phase-shifting microscopic interferometer (PSMI), phase steps are usually applied by moving one of the interferometer mirrors or the sample with a piezoelectric transducer (PZT). It is agreed[1–6] that one of the main error sources in PSMIs lies in accurately applying the predetermined phase steps using the actuator, whose sensitivity is usually unknown and tends to be nonlinear and dependent on variables such as its age, temperature, and some unexpected disturbances. Others[1,3,6,7] have suggested error-compensating algorithms, which implicitly evaluate the actual phase shifts at each point and use them to calculate the value of original phase difference between the interfering beams. An alternative approach is the phase-step-insensitive algorithms suggested by Farrel and Player[5] in which the computational effort required is much greater than in an ordinary fixed-step algorithm.

In this paper, we still use one of the most popular and easy to calculate algorithms,[4,8] i.e., the four-step technique, and feedback control is implemented for shifter asymptotic adjustment. In this way, we succeed in developing a PSMI without special requirements for its PZT and computing power. Comments on system design and experimental examples together with error analysis are also given.

2 Comments on the Mirau Interferometer

2.1 *Optical Arrangement for the Mirau Interferometer*

When considering the optical arrangement for the Mirau interferometer a compromise among aspects such as (1) the working distance needed, (2) the fabrication requirements for the optical components and their error contribution, and (3) mechanical complexity and stability should be made. Thus, the practical optimization of the optical arrangement for the Mirau interferometer is situation dependent.

The Mirau-type interferometer does have the disadvantage that it requires a long-working-distance microscope objective to accommodate an interferometer. However, in our case only 5×, 10×, and 20× objectives are considered, and further modification (removing their metal covers) has been done to reduce this problem (see Table 1).

Figure 1(a) is a widely used optical arrangement for the Mirau interferometer.[8–10] This two-plate configuration is simple, but the fabrication requirement for its reference plate is demanding because roughness on its back surface, in addition to its front surface, may have effects on the interferograms. This is true especially when the plate is thin. Moreover, perturbations in the optical path caused by its optical inhomogeneity and thickness also induce disturbances to the interferograms.

Figure 1(b) shows another optical arrangement[9,11] in which the back surface of the reference plate is used as reference and a compensator plate is inserted, which is necessary when white-light illumination is implemented. However, the mounting of the reference plate seems hard to cope with.

Figure 1(c) is the arrangement that we have adopted. The requirement for the reference plate in this configuration is reduced, although it appears somewhat complex when compared with the diagram in Fig. 1(a). There is no surface roughness requirement for its front surface, and perturbations in the optical path caused by its optical inhomogeneity and thickness are present in both arms of the Mirau interferometer and yield no net optical path difference when the two beams are combined. The effect on interference due to small perturbations in the optical path caused by the compensator plate can also be ignored,[9] and hence the low fabrication requirement for this additional plate of

Table 1 Working distance before and after modification and the depth of focus for the objectives with different magnification.

Magnification of Objective	Original Working Distance (mm)	Effective Working Distance (mm)	Depth of Focus (λ)
5×	9	23	99.5
10×	2.8	10.3	15.5
20×	1.5	3	5.7

 © 1996 Society of Photo-Optical Instrumentation Engineers
Downloaded From: https://www.spiedigitallibrary.org/journals/Optical-Engineering on 11/21/2018
Terms of Use: https://www.spiedigitallibrary.org/terms-of-use

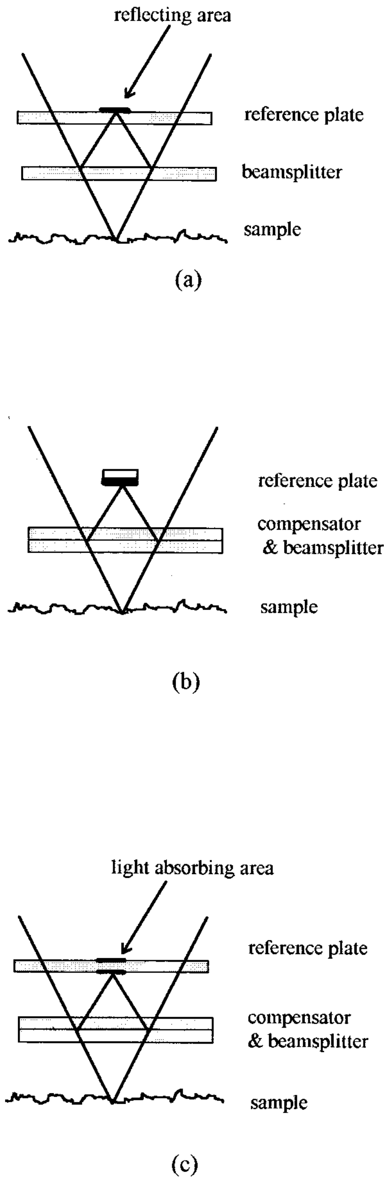

Fig. 1 Three kinds of optical arrangements for the Mirau interferometer.

the compensator. The problem of upward reflection from the reference plate is taken care of in our PSMI by smearing light-absorbing lacquer or ink onto the center area of its front surface.

Figure 2 shows a schematic diagram of our PSMI. To produce the phase shifting, the sample, which is attached to the PZT, moves. A disadvantage of this scheme is that the sample is likely to move out of focus for a high-magnification setup and therefore in other Mirau configurations the reference plate is normally phase shifted.[10] From Table 1, however, one can see that if the objective's magnification is below 40×, the depth of focus is so large that it makes no difference if the reference phase-shifting scheme or sample phase-shifting scheme is used. The main reasons we implemented the sample phase- shifting are that the PZT we had could not fit in the objective, and when the PZT is attached to the sample, the interferometer is somewhat simpler in structure and more stable.

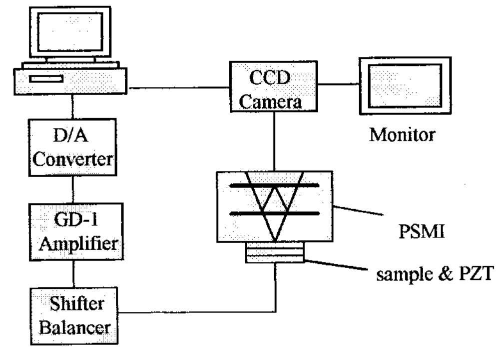

Fig. 2 Structural setup of PSMI for surface roughness measurement.

2.2 *Fringe Contrast and Data Sampling*

The phase error σ_ϕ due to quantization of irradiance into Q levels is given by[4,12]

$$\sigma_\phi = \frac{1}{\sqrt{3}\,\gamma_\tau Q}, \qquad (1)$$

where γ_τ is the fringe visibility or fringe contrast.

There are mainly three factors that may cause fringe contrast degradation in our PSMI: (1) bandwidth of illumination source, (2) central obstruction in objective, and (3) irradiance mismatch between the two interference beams.

When the bandwidth of the illumination source is considered, the interference pattern is given by[13,14]

$$I = I_0[1 + \gamma F(\mathrm{OPD}) \cos(2\pi \mathrm{OPD}/\lambda)], \qquad (2)$$

where

$$F(\mathrm{OPD}) = \begin{cases} \mathrm{sinc}\left(\dfrac{\pi \mathrm{OPD}}{\delta_c}\right), & \text{for a source of rectangle spectral distribution} \\ \exp\left[-\pi\left(\dfrac{\mathrm{OPD}}{\delta_c}\right)^2\right], & \text{for a source of Gaussian spectral distribution.} \end{cases}$$

Here OPD is the optical path difference between two interference beams, $\mathrm{sinc}(x) = \sin(x)/x$, and the coherence length δ_c is defined as $\lambda^2/\Delta\lambda$. Hence, the only effect of integrating over the wavelength bandwidth is to reduce the modulation of the interference fringes by a factor $F(\mathrm{OPD})$.

In our PSMI, a white-light source and a spectral filter ($\lambda = 630$ nm, $\Delta\lambda = 8$ nm) are used for illumination just as in other schemes.[13,14] For an OPD of 2 μm, the modulation is reduced to 0.997 for a source with rectangular spectral distribution and to 0.995 for a source with Gaussian spectral distribution, thus the fringe contrast degradation due to illumination spectrum can be ignored.

Downloaded From: https://www.spiedigitallibrary.org/journals/Optical-Engineering on 11/21/2018
Terms of Use: https://www.spiedigitallibrary.org/terms-of-use

Table 2 Reflection coefficient of components in the Mirau interferometer required by Eq. (3).

	R_s	R_b	R_r
Coating surface	100%	50%	100%
Optical disk	80%	47%	100%
Other surface	50%	41%	100%
Ordinal optical surface	4%	17%	100%

The second contrast degradation factor is the central obstruction in objective especially for a large field of view.[9] In our system, the central obstruction ratio ϵ is only ~ 0.1 and the field of view is $\sim 0.256\times 0.256\ \text{mm}^2$, thus its effect on contrast degradation can also be ignored.

Because irradiance mismatch can cause contrast degradation, the reflection coefficient of components in the interferometer should obey the following relationship to keep high fringe visibility, i.e.,

$$(1-R_b)^2 R_s = R_b^2 R_r , \tag{3}$$

where R_b is the reflection coefficient of beamsplitter front surface, and the back surface is assumed to have a 100% transmission coating; R_s is the reflection coefficient of sample; R_r is the reflection coefficient of reference surface; and the compensator is supposed to be coated with 100% transmission film on both surfaces. Table 2 shows the coefficients of components that are required for different samples according to Eq. (3).

The product $\gamma_\tau Q$ in Eq. (1) represents the modulated portion of the irradiance and is inversely proportion to the phase error σ_ϕ. Therefore the fringe irradiance should cover as much of the detector's dynamic range as possible and the data sampling of interference fringes should have sufficient quantization levels so as not to significantly reduce the signal modulation.[3,4,10,12]

2.3 *Temporal Coherence Property*

Roughness testing of very thin transparent glass flats is usually difficult for a laser system because the light reflected from the back surface can interfere with the reference beam and with the light reflected from the front surface, making it impossible to determine the roughness of one surface from the resulting interferograms. Therefore the temporal coherence property of the light source should be tailored such that the light reflected from the back surface is incoherent to the light reflected from the front surface and from the reference surface.

We assume that spurious fringes from the back surface are suppressed if they show a contrast of $\gamma_\tau = \gamma F(\text{OPD}) < 0.01$, where γ is the contrast due to other factors. Assuming $\gamma = 1$, then from Eq. (2) we get $\text{OPD} > 49\,\mu\text{m}$ for our source ($\lambda = 630$ nm, $\Delta\lambda = 8$ nm) with rectangle spectral distribution and $\text{OPD} > 60\ \mu\text{m}$ with Gaussian spectral distribution.

The OPD caused by the thickness of sample in the Mirau objective can be expressed as

$$\text{OPD} = 2n\Delta + D(x^2 + y^2), \tag{4}$$

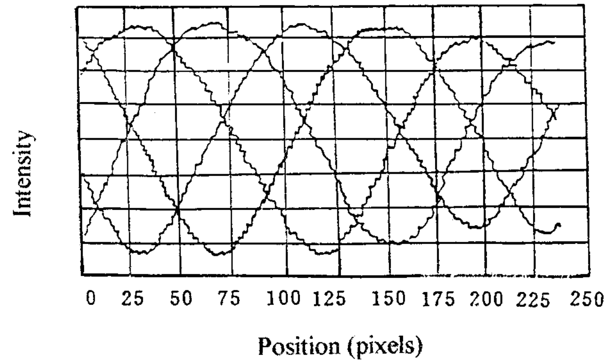

Fig. 3 Sequence of four irradiance profiles and their relative locations.

where x and y are the coordinates in the field of view, D is the defocusing quadratic factor; and Δ and n are the thickness and refractive index of sample, respectively. Thus, the minimum OPD in the field of view is $2n\Delta$. Assuming $n = 1.5$, then the minimum thickness of sample must be over 20 μm [60/(2 × 1.5)] so as to cancel out undesired interference.

3 Intelligent Phase-Shifting Control

3.1 *Determination of Phase Shifts and Shift Errors*

Techniques for determining the phase shift value has been reviewed in other papers.[3,5] Here we implement a somewhat similar technique, which involves extracting a sequence of irradiance profiles across fringes from the smooth-processed interferograms (see Sec. 3.2) and locating the peak-value points by a scanning comparison (described later) along these cosinelike profiles so as to determine the amount of each phase shift.

Referring to Fig. 3, after four successive cosinelike profiles are extracted, the peak-value points are located, then by comparing the location shifts with the periodicity of peak-value points it is easy to determine phase shifts and their errors.

Peak-value points can be determined by a scanning comparison along the profile, that is if

$$(I_{m-1}+I_m+I_{m+1})-(I_{m-2}+I_{m-1}+I_m)=I_{m+1}-I_{m-2}\geqslant 0, \tag{5a}$$

and

$$(I_m+I_{m+1}+I_{m+2})-(I_{m-1}+I_m+I_{m+1})=I_{m+2}-I_{m-1}\leqslant 0, \tag{5b}$$

then point m is a peak-value point. Here I_m represents irradiance value of point m.

The calculation time can be greatly reduced if we perform the scanning comparison only for points whose irradiance is over a specific threshold.

3.2 *Preprocessing of Interferograms*

From Sec. 3.1 we know that the irradiance profiles are used to determine the phase shift and shift errors. However, the

Downloaded From: https://www.spiedigitallibrary.org/journals/Optical-Engineering on 11/21/2018
Terms of Use: https://www.spiedigitallibrary.org/terms-of-use

ripples in the irradiance profiles due to the surface roughness usually make the location of profiles and determination of phase shift confusing. Therefore it is necessary to smooth the interferograms first.

In our PSMI, a window-convolution technique[15] is introduced for the smoothing process according to the following equation:

$$I'(x,y)=\frac{\sum_{i=x-1}^{x+1}\sum_{j=y-1}^{y+1}W(i-x+2,j-y+2)I(i,j)}{\sum_{i=1}^{3}\sum_{j=1}^{3}|W(i,j)|}, \quad (6)$$

where $I(x,y)$ is the original irradiance at point (x,y); $I'(x,y)$ is the result after smoothing; and $W(i,j)$ is the weight in the convolution window, whose form has some dependence on sample condition.

We choose the size of the convolution window in terms of the lateral resolution unit of the objective, which is given by[16]

$$\delta\sim 0.59\lambda/\mathrm{NA}, \quad (7)$$

where the central obstruction in the objective is $\epsilon\sim 0.1$, and NA is the numerical aperture.

The number of data points sampled in terms of lateral resolution units is given by

$$N=(D_s\delta)^2, \quad (8)$$

where D_s represents the data sampling density, whose value as determined from precalibration is about 2 pixels/μm for the 10× objective.

Substituting $\lambda=630$ nm and NA=0.25 into Eq. (7) we get $\delta=1.48$ μm. Then from Eq. (8), we obtain $N=9$. Therefore a 3×3-pixel convolution window is used for preprocessing.

Furthermore, if the sample is a rough surface, then an average of several section profiles in the interferogram is further needed to get a smoother irradiance profile.

3.3 *Shifter Asymptotic Adjustment by Feedback Control Method*

Referring to Fig. 2, a computer is used to control the phase-shifting process according to a stored digital signal array, which is converted to an amplitude signal array by a digital-to-analog converter (DAC) and magnified by a GD-1 high-voltage amplifier before entering a shifter balancer for PZT movement control.

After phase shift errors are obtained by the technique described in Sec. 3.1, every acceptable frame corresponding to the phase step with a shift error smaller than the predetermined value is stored, and feedback signals that are proportional to shift errors are used to amend the existing digital signal array for succeeding sequence of phase shifting. This procedure continues until we obtain at least one desired phase shift for each phase step whose residual error is small enough to be satisfactory. As an example Table 3 shows the typical status of our shifter corresponding to each step in multiple sequence of phase shifting, where √ represents a desired phase shift and × represents an undesired phase shift.

Table 3 Typical status of shifter corresponding to the frames acquired in multiple sequence of phase shifting.

Phase shift	Step 1	Step 2	Step 3	Step 4
1	√	×	×	×
2	√	×	×	√
3	√	√	√	×

In practical calculation, all acceptable frames corresponding to the same phase step can be averaged for further error reduction[1] so that every effective frame in the multiple sequence of data acquisition is used without waste.

In our PSMI, the time constant for acquisition of one sequence of frames after data processing and PZT setting is about 15 s. During this interval, fringe drift usually occurs because of thermal drift, system vibration and hysteresis of the PZT. Therefore the setting of the PZT is crucial in our PSMI, and this is realized by careful feedback control in the way already described. Thus, in Table 3 the first frame of each sequence of phase shifting is always acceptable.

4 Experiment Examples

Figure 4 shows a measurement of an optical surface while its interferogram is being made, and the distribution of surface profile departure density, i.e., the height histogram and the interferogram are shown in Figs. 5(a) and 5(b), respectively. The effect of the phase shifter feedback control on the measurement results is clearly demonstrated in Table 4.

Table 5 shows the repeatability results for measurements on a porcelain surface that is used as a vacuum sealing device. The interferogram and the corresponding height histogram are shown in Figs. 6(a) and 6(b).

Fringe pattern irregularities can be seen in Fig. 6(a), and thus the height histogram is no longer of normal distribution, but has a distribution with higher density in the negative and positive directions. Therefore the porcelain surface load-bearing area is small, and cannot be a good sealing device. In comparison, we can see that in Fig. 5(a) there are no fringe pattern irregularities, and hence its height histogram is in the form of a normal distribution.

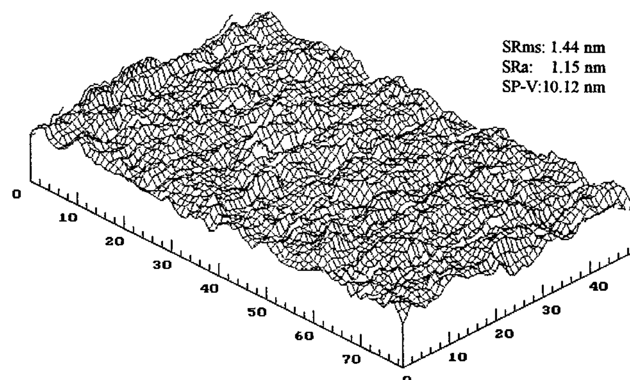

Fig. 4 Three-dimension view of the optical test surface.

Downloaded From: https://www.spiedigitallibrary.org/journals/Optical-Engineering on 11/21/2018
Terms of Use: https://www.spiedigitallibrary.org/terms-of-use

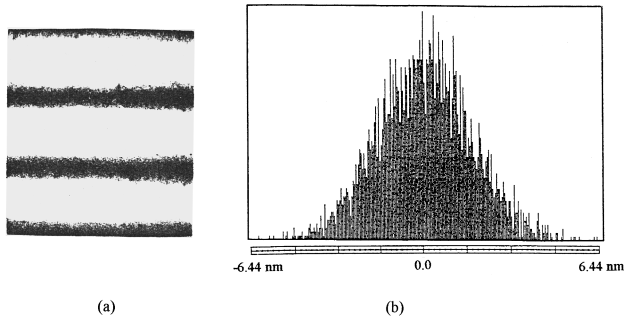

Fig. 5 (a) Interferogram and (b) height histogram for an optical test surface.

5 Error Analysis

5.1 *Error due to Roughness of Reference Mirror σ_r*

The roughness of the reference surface in our PSMI was precalibrated against a supersmooth silicon substrate, whose roughness is of ~0.25 nm, thus all measurement results contain a calibration error, which is $\sigma_r = 0.25$ nm.

5.2 *Error due to System Adjustment σ_a*

Phase distribution $\phi(x,y)$ in our PSMI can be expressed by

$$\phi(x,y) = \phi_0(x,y) + \sigma_a, \tag{9}$$

for $\sigma_a = Ax + By + C + D(x^2 + y^2)$, where $\phi_0(x,y)$ is the original phase distribution due to height variation, and $Ax + By$ and $C + D(x^2 + y^2)$ are tilting term and defocusing term, respectively, due to the adjustment error.

The adjustment error σ_a on the right-hand side of Eq. (9) can be canceled out by least-squares fitting, so it is ignored in our discussion, i.e., $\sigma_a = 0$.

5.3 *Error due to Phase Shifter σ_ϕ*

Supposing that there are N sampling points in one fringe period, which corresponds to phase shift of $\lambda/2$, the control accuracy ϵ_c of the feedback system is assumed to be

$$\epsilon_c = \lambda/2N. \tag{10}$$

By substituting $N = 200$ and $\lambda = 630$ nm into Eq. (10) we get $\epsilon_c \approx 1.6$ nm. Thus the error due to the phase shifter can be considered to be $\sigma_\phi = 0.1\ \epsilon_c = 0.16$ nm.

Table 5 Repeatable roughness measurement results for a vacuum porcelain surface.

	SRms (nm)	SRa (nm)	SP-V (nm)
Measurement 1	19.72	9.16	148.33
Measurement 2	19.34	9.12	145.05
Measurement 3	18.97	8.94	142.28
Repeatability	0.30	0.10	2.47

5.4 *Quantization Error σ_q*

The quantization error[4,12] due to DAC is given by Eq. (1). Here $Q = 2^8 = 256$, $\gamma_\tau = 0.5$, and $\lambda = 630$ nm, thus we obtain $\sigma_q = 0.28$ nm; this can also be used as the height resolution of our PSMI.

5.5 *Error due to Calculation Equation σ_e*

In our PSMI, the height variation distribution is calculated from

$$h(x,y) = (\lambda/4\pi)\phi(x,y). \tag{11}$$

This relationship, however, is valid only for normal incidence illumination. For oblique illumination the preceding relationship should be modified and expressed as[11]

$$h(x,y) = \eta(\lambda/4\pi)\phi(x,y), \tag{12}$$

where the correction factor η due to oblique illumination has a value of about 1.016 for a 10× objective from Ref. 11.

Thus the error in the calculation according to Eq. (11) is given by

$$\Delta h(x,y) = (\eta - 1)(\lambda/4\pi)\phi_{\max}. \tag{13}$$

Assuming $\phi_{\max} = \pi/10$, the error is $\sigma_e = \Delta h(x,y) = 0.25$ nm.

5.6 *Error due to Vibration σ_v*

Although our PSMI is a quasi-common-path system, vibration sources such as the air-conditioning system, people walking about, and acoustical noise will make the analysis of supersmooth surfaces unrepeatable and cause a sinusoidal phase error just like the shifter miscalibration.[3,4] Therefore, methods used to suppress the phase shifter error discussed in Sec. 3 can also be implemented here, and it is reasonable to suppose $\sigma_v = \sigma_\phi = 0.16$ nm.

Table 4 Test results for an optical surface with feedback control on and off.

Feedback On			Feedback Off		
SRms (nm)	SRa (nm)	SP-V (nm)	SRms (nm)	SRa (nm)	SP-V (nm)
2.24	1.81	15.05	1.44	1.15	10.12

SRms is the root mean square in S; SRa is the average roughness in S; and SP-V is the peak-to-valley difference in S. Here S represents the 2-D sampling surface.

Downloaded From: https://www.spiedigitallibrary.org/journals/Optical-Engineering on 11/21/2018
Terms of Use: https://www.spiedigitallibrary.org/terms-of-use

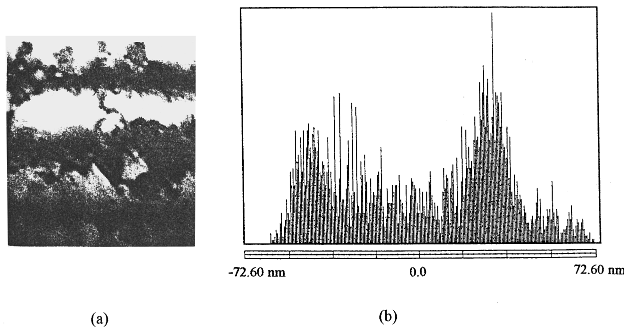

Fig. 6 (a) Interferogram and (b) height histogram for a vacuum porcelain surface.

From the preceding, we conclude that the total test error σ_τ is

$$\sigma_\tau = (\sigma_r^2 + \sigma_a^2 + \sigma_\phi^2 + \sigma_q^2 + \sigma_e^2 + \sigma_v^2)^{1/2}. \tag{14}$$

Substituting the preceding values into Eq. (14), we obtain $\sigma_\tau = 0.5\,\text{nm}$.

6 Conclusion

We have developed a PSMI based on Mirau interferometer with actual height resolution of ~0.3 nm and measurement accuracy of ~0.5 nm.

In the development of the Mirau interferometer, a compromise among aspects such as (1) the working distance needed, (2) fabrication requirement for the optical components and their error contribution, and (3) mechanical complexity and stability has been made.

To obtain the correct phase step for the four-step technique, multiple sequences of frames are taken with asymptotic adjustment of the shifter.

Analysis of the height histogram is a useful and easy way to evaluate the surface quality and some relative physical properties.

Acknowledgment

This work is supported by the Chinese Academy of Sciences and supervised by Prof. Fuxi Gan. The authors thank Ms. Liuhong Huang for her help in the testing work and Prof. Jianlin Chao for providing the polished silicon samples.

References

1. J. Schwider, R. Burow, K.-E. Elssner, J. Grzanna, R. Spolaczyk, and K. Merkel, ''Digital wave-front measuring interferometry: some systematic error sources,'' *Appl. Opt.* **22**(21), 3241–3432 (1983).
2. J. Schwider, ''Advanced evaluation techniques in interferometry,'' in *Progress in Optics*, Vol. XXIX, E. Wolf, Ed., pp. 271–359, Elsevier Science Publishers, Amsterdam (1990).
3. K. Creath, ''Phase-measurement interferometry techniques,'' in *Progress in Optics*, Vol. XXVI, E. Wolf, Ed., pp. 351–393, Elsevier Science Publishers, Amsterdam (1988).
4. K. Creath, ''Phase-measurement interferometry: *beware* these errors,'' *Proc. SPIE* **1553**, 213–220 (1991).
5. C. T. Farrel and M. A. Player, ''Phase-step insensitive algorithms for phase-shifting interferometry,'' *Meas. Sci. Technol.* **5**, 648–652 (1994).
6. Y. Y. Cheng and J. C. Wyant, ''Phase shifter calibration in phase-shifting interferometry,'' *Appl. Opt.* **24**(18), 3049–3052 (1985).
7. P. Hariharan, B. F. Oreb, and T. Eiju, ''Digital phase-shifting interferometry: a simple error-compensating phase calculation algorithm,'' *Appl. Opt.* **26**(13), 2504–2506 (1987).
8. J. C. Wyant, ''Interferometric optical metrology: basic principles and new systems,'' *Laser Focus* **18**(5), 65–71 (May 1982).
9. B. Bhushan, J. C. Wyant, and C. L. Koliopoulos, ''Measurement of surface topography of magnetic tapes by Mirau interferometry,'' *Appl. Opt.* **24**(10), 1489–1497 (1985).
10. User's manual for TOPO-2D two-dimensional noncontact surface profiler, WYKO Corp. of Tucson (Apr. 1987).
11. J. F. Biegen, ''Calibration requirements for Mirau and Linnik microscope interferometers,'' *Appl. Opt.* **26**(11), 1972–1974 (1989).
12. C. P. Brophy, ''Effect of intensity error correlation on the computed phase of phase-shifting interferometry,'' *J. Opt. Soc. Am. A* **7**(4), 537–541 (1990).
13. K. Creath, ''Step height measurement using two-wavelength phase-shifting interferometry,'' *Appl. Opt.* **26**(14), 2810–2816 (1987).
14. H. H. Hopkins, ''The theory of coherence and its applications,'' in *Advanced Optical Techniques*, A. C. S. van Heel, Ed., North Holland Publishing, Amsterdam (1967).
15. P. H. Schroer and J. Becker, ''Computer automation for scanning tunneling microscopy,'' *IBM J. Res. Develop.* **30**, 543–548 (1986).
16. M. Born and E. Wolf, ''Elements of the theory of diffraction,'' Chap.8 in *Principles of Optics*, pp. 370–458, Pergamon Press, Oxford (1975).

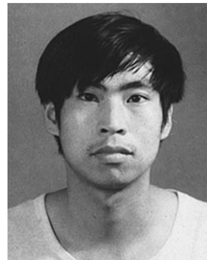

Zhihua Ding received the BS degree from the Optical Instrument Engineering Department of Zhejiang University in 1989 and was an assistant engineer with the Factory for Comprehensive Exploitation of Stone-coal in Kaihua, Zhejiang Province, for 2 years. He is currently a PhD candidate in the Shanghai Institute of Optics and Fine Mechanics. His current interests are microscopy, optical testing, and near-field optics.

Guiying Wang graduated from the Department of Physics of Nankai University in Tian Jing. She has engaged in research of numerical simulation of light beam propagation, holography, digital image processing, and optoelectronics and is now working on optical precision testing.

Zhijiang Wang is an academician of the Chinese Academy of Sciences and is a renowned expert in optics and optoelectronics in China.

Downloaded From: https://www.spiedigitallibrary.org/journals/Optical-Engineering on 11/21/2018
Terms of Use: https://www.spiedigitallibrary.org/terms-of-use